Penetration of Buoyant Coastal Discharge onto the Continental Shelf: A Numerical Model Experiment

RICHARD W. GARVINE

The Graduate College of Marine Studies, University of Delaware, Newark, Delaware

(Manuscript received 12 May 1998, in final form 1 October 1998)

ABSTRACT

Plumes of buoyant water produced by inflow from rivers and estuaries are common on the continental shelf. Typically they turn anticyclonically to flow alongshelf as buoyancy-driven coastal currents. During this passage, mixing with ambient shelf water gradually erodes the plume buoyancy so that its alongshelf penetration is finite. This paper addresses the extent of this penetration and how it is determined by fundamental dimensionless flow parameters.

A three-dimensional numerical model is applied to an idealized flow regime. Ambient shelf conditions include tidal motion, but neither wind stress nor ambient alongshelf current. The alongshelf extent of penetration is evaluated after the plume reaches a stationary condition downshelf. A total of 66 model experiments are conducted, including variations in buoyant source and ambient shelf properties. Five dimensionless parameters determine the alongshelf and across-shelf penetration, the latter the coastal current width. The most critical of these is τ, the source volume transport scaled by the associated source geostrophic transport. For fixed shelf bottom slope and no tides, similarity forms are found for both alongshelf and across-shelf penetration for a wide range of τ. Increased shelf bottom slope and increased shelf tidal amplitude shorten the alongshelf penetration.

The vertical turbulent closure scheme itself contributes one of the five model parameters, the background eddy viscosity or diffusivity. This background viscosity ν is added to the viscosity determined from the Mellor–Yamada level 2.5 closure scheme to give N, the vertical viscosity used by the model. Where the local Richardson number exceeds about 0.2, as in most buoyant plumes, the Mellor–Yamada scheme ''switches off,'' forcing N to default to ν. Plume penetration properties thus are found to depend significantly on ν. At present one must choose ν arbitrarily, thus introducing uncertainty into the model results.

1. Introduction

Plumes of buoyant water are common features on the continental shelf. Typically they are produced by the inflow from a coastal buoyancy source, such as a river or estuary. After entering the shelf regime, they usually turn anticyclonically toward the direction of coastally trapped wave propagation (''downshelf'' in the usage of this paper) and continue penetration alongshelf as buoyancy-driven coastal currents. These gradually terminate as mixing with ambient shelf water erodes the buoyancy. Well-known examples include the Norwegian coastal current (Mork 1981), the Columbia River plume (Hickey et al. 1998), and the Delaware coastal current (Münchow and Garvine 1993). There is an extensive literature on buoyant plumes in shelf water, including observational, laboratory model, and mathematical (including numerical) model studies. Hill (1998) gives an excellent review of buoyancy effects in coastal and shelf seas.

In this paper, the focus is on an unstudied but important property of buoyant plumes and coastal currents in shelf water. What is the extent of alongshelf penetration for a steady coastal buoyancy source? How does this downshelf penetration vary with properties of the discharge and ambient shelf? Can one predict the downshelf penetration, given the fundamental properties? What is the extent of across-shelf penetration? In particular, can one predict the width of the buoyancy-driven coastal current?

If there is no mixing between inflowing buoyant water and ambient shelf water, the answer to the first question is simple. For a steady source, the extent of downshelf penetration would be unbounded and the coastal current would have no end. It would form a closed circuit bounding the land mass that gave rise to the source. Thus, the finite extents that are observed depend explicitly on mixing processes. A study of downshelf penetration is inherently a study of mixing processes on the continental shelf.

Knowledge of the downshelf extent of penetration has a variety of uses. The dynamics of buoyancy-driven

Corresponding author address: Dr. Richard W. Garvine, The Graduate College of Marine Studies, University of Delaware, Robinson Hall, Newark, DE 19716-3501.
E-mail: rgarvine@udel.edu

coastal currents depends upon the alongshelf pressure gradient present. This, in turn, depends upon the alongshelf scale for the buoyancy itself. The dynamics is thus strongly coupled to the mixing. The extent of penetration determines the advection scale downshelf for coastal and estuarine species that have planktonic larvae. Such larvae will tend to be transported downshelf by the coastal current away from the site of their origin, unless other processes intervene. A common example is the Atlantic blue crab, *Callinectes sapidus,* that spawns in the mouths of estuaries on the U.S. East Coast (Epifanio 1996). Anthropogenic inputs into coastal waters often enter through rivers and estuaries. Their range downshelf will thus often be determined by the penetration distance for buoyant flows.

Buoyancy-driven coastal currents often exert major control over the large-scale, mean circulation of continental shelves. Chapman and Beardsley (1989) have suggested a particularly large downshelf extent for the mean flow developed from Arctic buoyancy sources. They hypothesize that a large extent of the shelf circulation on the east coast of North America has its origin in Arctic sources of cold, but fresher, and therefore lighter water. The particular sources they suggest are the West Greenland Current and the flow exiting Hudson Strait. Collectively, these lighter waters, perhaps augmented by the Baffin Island Current, form the Labrador Current, then continue generally south and westward, reinforced by local coastal buoyancy sources. Much of this flow continues on the Scotian shelf and finally appears as the mean southwestward flow in the Middle Atlantic Bight. Such a continuous coastal current would be over 5000 km long. One application of the present model study of downshelf penetration would be to assess the extent of penetration of such Arctic sources so as to test the hypothesis of Chapman and Beardsley (1989).

Downshelf penetration has been examined as part of two laboratory model experiments. Griffiths and Hopfinger (1983) released a fixed volume of buoyant water from behind a lock at one end of a rotating channel. By extrapolating the decay in velocity of the leading nose of the resulting density current along the vertical channel wall they estimated the downstream penetration distance at which the current would have been arrested. They found the penetration to depend on the Rossby radius and the surface area of the buoyant water prior to release. The present work, in contrast, employs continuous (steady) inflow of buoyant water. Whitehead and Chapman (1986) used a continuous release to study the propagation of buoyant currents along a sloping shelf. Using a similar extrapolation technique, they estimated downshelf penetration distances and found them to be about 27 Rossby radii.

The approach taken in this study is to use a primitive equation model that includes a standard turbulent closure submodel and apply it to a simplified, idealized setting. The model shelf is long and straight with constant bottom slope. Shelf water is of uniform density and, apart from tidal motion, unforced by wind stress or ambient alongshelf current. (The effect of these two latter forcing agents will be the subject of a future paper.) The buoyancy source is steady with a simple configuration. The intent is to model the climatic mean alongshelf and across-shelf penetration for a particular coastal buoyancy source.

My method is patterned after laboratory studies in fluid dynamics. A large number of different model runs having different model parameters are conducted, such as source volume flux and source buoyancy. The goal is to find how the downshelf and across-shelf penetration vary with the fundamental parameters of the flow problem. An associated goal is to synthesize the model results so as to achieve what fluid dynamicists call dynamic similarity (Kundu 1990), where universal dependence of a flow property, such as downshelf penetration, is rendered as an empirical function of a small number of dimensionless parameters.

The paper is organized as follows. Section 2 describes the model used. Section 3 introduces the model parameters. Section 4 treats the plume properties for the standard case that is used as a central reference for a large variety of experiments. Section 5 presents results for a variety of buoyancy forcing, while section 6 treats variations in ambient shelf conditions, including tides. Section 7 concludes the paper.

2. Model description

The model used here is ECOM3d, a particular version of the model developed by Blumberg and Mellor (1987), sometimes called the Princeton Ocean Model. It is a primitive equation, finite-difference model that treats time-dependent flows in three dimensions. The vertical momentum balance is hydrostatic and a free surface is incorporated. The latter is important to the present application that includes barotropic tidal circulation with its consequent advection and mixing. Because the model has been frequently used, I omit stating the governing equations, but the interested reader will find them in Kourafalou et al. (1996).

The model geometry appears in Fig. 1. The coordinates x, y form a Cartesian pair with x alongshelf and y across-shelf. The Coriolis parameter f is set constant because the scale is not large. Hence, the geographic orientation of the coastline ($y = 0$) is unimportant. The model uses a sigma coordinate transformation for the vertical

$$\sigma = \frac{z - \eta}{h + \eta},$$

where z is the vertical coordinate, η is the free surface height, and h the local still water depth. Thus, σ ranges from zero at the free surface to -1 at the bottom.

The dependent variables are the three components of velocity, u, v, w, η, temperature, salinity S, and two

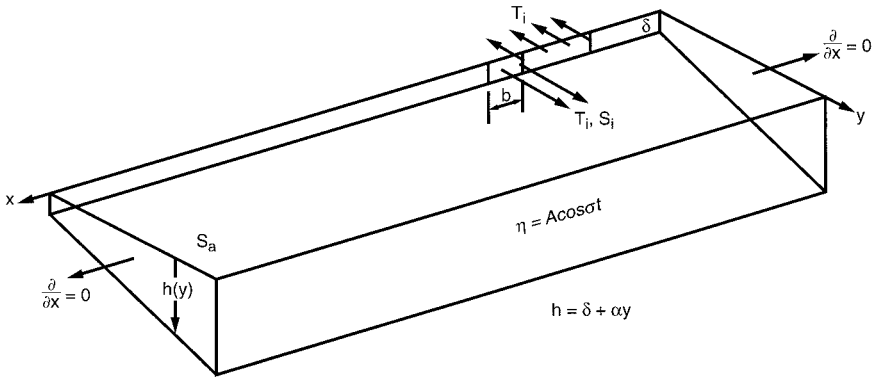

FIG. 1. Sketch of the model configuration. The view is of a section of the continental shelf from above and seaward. The coast lies along the x axis. The shelf bottom is planar with constant bottom slope α in the across-shelf (y) direction. The inlet for buoyant source water has breadth b and depth δ from which comes water of salinity S_i and volume transport T_i. Upshelf of the inlet is an outlet, also of volume transport T_i. Shelf water has uniform salinity S_a. Smooth boundary conditions ($\partial/\partial x = 0$) are imposed at both open, across-shelf boundaries, while tidal height variations are imposed on η at the open, seaward boundary.

properties of the turbulence field: turbulent macroscale and turbulent kinetic energy. Density ρ is computed from the equation of state. These variables are computed by the model using the continuity equation, the two horizontal momentum equations, and two equations for the advection–diffusion of heat and salt.

The model uses the level 2.5 turbulent closure submodel of Mellor and Yamada (1982) to compute the vertical eddy viscosity N. Vertical diffusivity is set as $D = N$ (turbulent Prandtl number = 1). The submodel employs a minimum or background viscosity level ν. Except for one set of numerical experiments, $\nu = 5 \times 10^{-6}$ m^2 s^{-1} is used. For numerical stability, the model requires finite horizontal eddy viscosity N_H and diffusivity D_H. I equated these and used the scheme of Smagorinsky (1963) to compute N_H, choosing the empirical coefficient $C_a = 0.1$. This led to computed values for N_H of about 10 m^2 s^{-1}.

For the present application where steep gradients in salinity are common, use of the standard central difference scheme for the advection of salt will introduce artifacts. To avoid this, I used the recursive scheme of Smolarkiewicz and Grabowski (1990), even though it doubled the time of computations.

Boundary conditions imposed at the free surface are zero stress (wind stress is absent) and zero flux of salt and heat. At the bottom, heat and salt fluxes are again zero, while bottom stress is computed from the standard quadratic form with drag coefficient c_d taken as the larger of 0.0025 or $0.16/(\log\Delta z/z_0)^2$, where $z_0 = 0.3$ cm is the roughness height and Δz is the height above bottom half way to the next σ level.

The model domain (Fig. 1) represents an idealized continental shelf with constant bottom slope α in the across-shelf direction; the coastline ($y = 0$) and all isobaths parallel the x axis. The water depth at the coast is δ, set at 10 m. The inlet and outlet configurations are selected to model the subtidal flow fields observed at the mouths of major estuaries in the Northern Hemisphere, such as Delaware Bay (Garvine 1991). Inflow onto the shelf is present over the alongshelf distance b, while, to the right looking onshore, outflow of ambient or mixed water is present over the adjacent, upshelf distance of $2b$. Across the inlet, $v = v_i$, $S = S_i$ uniformly over the breadth b and depth δ. Across the outlet, $v = -v_i/2$, so that the net volume transport onto the shelf is zero. The temperature of the entire domain, including the inlet, is constant at 10°C so that all buoyancy differences result from salinity differences through the nonlinear equation of state. Elsewhere along the coast, the solid coastal wall is present. There the boundary conditions are $u = v = 0$ and heat and salt flux are zero.

The offshore, open boundary is set at $y = L$, usually at about 70 km from the coast. In general, flow disturbances from coastal buoyancy forcing are limited to a few internal Rossby radii, or about 20 km, so the offshore boundary imposes little constraint on the motion inshore. The principal function of this boundary is to impose tidal forcing on the inner shelf. Here the tidal height is imposed uniformly in x as

$$\eta(L,t) = A\cos\sigma t,$$

where $\sigma = 2\pi/P$; P is the M_2 tidal period, 12.42 h; and A the amplitude. For cases where only buoyancy forcing is present, $A = 0$. Corresponding velocities u and v are then computed from the tidal height using linearized momentum equations.

Two open, across-shelf boundaries complete the model domain. These are located sufficiently far from the inlet that the direct effects of buoyancy forcing do not reach them. The boundary conditions used were the so-called smooth boundary conditions where the normal, or x, derivatives of η and of the vertically averaged

horizontal velocity were set to zero. This implementation passed two critical tests. It led to barotropic tidal flow fields that were invariant alongshelf when buoyancy forcing was absent and it permitted buoyancy-driven coastal currents to flow smoothly across the downshelf model boundary in test cases.

The initial flow state is one of rest with $S = S_a = 32$ and temperature 10°C, representing ambient shelf water with no stratification. The inlet flow and tidal forcing are zero initially and increase with time using a ramp function of length 6 hours. The model uses a split time step with a short time step for the external or barotropic mode, based on the CFL condition, and a much longer internal mode time step. For the latter I used 894.24 $s = P/50$, but smaller values when shelf tides were imposed. Generally the external time step was a factor of 40 shorter.

The horizontal grid is rectangular with a mesh size of 1.5 km near the inlet, sufficient to resolve the internal Rossby radius, which is typically 8 km. To achieve better efficiency I stretched the grid in the y direction using an exponential function and in the x direction away from the inlet using a cosh function. Typically, there are 400 grid points in x and 40 in y, but some configurations have 500×50. Runs with double horizontal mesh size give similar results, apart from a lack of fine detail. There are 21 points in the vertical with increased resolution near the bottom and near the free surface with a minimum vertical interval of 0.2 m.

3. Model parameters

The flow field outcomes will be formally determined by the seven dimensional parameters: inlet breadth b, Coriolis parameter f, inlet (and coastal wall) depth δ, inlet salinity difference $S_a - S_i$ (or density anomaly $\rho_a - \rho_i$), inlet velocity v_i, tidal amplitude A, and bottom slope α. For convenience, the reduced gravity $g' = (\rho_a - \rho_i)g/\rho_a$ was used in place of the density anomaly, and the inlet transport $T_i = b\delta v_i$ in place of v_i. These seven parameters carry two independent dimensions, length and time. The Buckingham Pi theorem (Kundu 1990) then states that there are formally $7 - 2 = 5$ independent, dimensionless model parameters that may be formed from these seven that determine the results.

The primary parameter is the scaled inlet transport (Garvine 1987)

$$\tau = \frac{2T_i f}{g'\delta^2}.$$

Thus τ gives the inlet transport scaled by the transport $T_g = g'\delta^2/(2f)$, the amount of geostrophic transport associated with the shear generated by a Margules density front of strength g' ranging over the depth scale δ. We may expect τ to exert a strong influence over the far downshelf part of the plume, as that part should depend strongly upon the total rate of inflow.

The second parameter is the inlet Kelvin number

$$K_i = b/r_i,$$

where $r_i = c_i/f$ is the internal Rossby radius relative to inlet conditions with c_i the internal wave phase speed given by

$$c_i = \sqrt{g'\delta}.$$

Thus, K_i measures the inlet scale in Rossby radii. We may expect K_i to determine especially the near field of the plume, that is, within a few Rossby radii of the inlet. For K_i small, the near-field flow should behave as if it were nonrotating (Garvine 1987). This outcome could occur at midlatitudes for small-scale plumes, such as from power plant discharges or narrow coastal streams or from large-scale, natural plumes near the equator. For K_i of order unity, rotation should be important throughout the plume.

Alternative parameters to τ and K_i are the inlet Froude number $F_i = v_i/c_i$ and the inlet Rossby number $\mathrm{Ro}_i = v_i/(fb)$. Here these are given by $F_i = \tau/(2K_i)$ and $\mathrm{Ro}_i = \tau/(2K_i^2)$.

The parameters τ and K_i characterize the buoyancy source. The next two characterize the ambient shelf flow. One is just the shelf bottom slope α; the other is the scaled tidal amplitude

$$\epsilon = A/\delta.$$

In tidal circulation theory ϵ measures the degree of tidal nonlinearity (Ianniello 1977).

The fifth parameter is the inlet aspect ratio b/δ. For these experiments this parameter is always large, the order of 10^3, so that typical variations should not exercise control over the flow field. However, for laboratory experiments where b/δ might be order one, it could play a major role.

The physical problem should be set by the five dimensionless parameters: τ, K_i, α, ϵ, and b/δ, with the latter having only weak control. The model itself, however, introduces two other independent parameters through its subgrid-scale parameterizations: the background vertical eddy viscosity ν and the horizontal viscosity coefficient C_a in the Smagorinsky (1963) scheme. In principle, the flow dynamics and mixing should not depend upon these parameters. One would expect the Mellor–Yamada closure scheme to produce $N \gg \nu$ and the Smagorinsky scheme to produce levels of $N_H = D_H$ that maintain numerical stability but are too small to do effective mixing. Nevertheless, as illustrated in the next section, for a wide range of parameter space the Mellor–Yamada scheme gives zero turbulent components in the stratified plume. As a consequence, both ν and C_a values can affect the entire flow field. A convenient dimensionless form for ν is the Reynolds number

$$\mathrm{Re} = \delta c_i/\nu.$$

In later sections it will be shown how the across-shelf and alongshelf penetration of the buoyant coastal discharge varies with these parameters. But first I examine

TABLE 1. Standard case parameter values.

Parameter	Name	Value
f	Coriolis parameter	0.937×10^{-4} s^{-1}
b	Inlet breadth	12 km
δ	Inlet depth	10 m
$S_a - S_i$	Inlet salinity difference	7
v_i	Inlet velocity	0.00417 m s^{-1}
T_i	Inlet volume transport	500 m^3 s^{-1}
A	Tidal height amplitude	0
g'	Inlet reduced gravity	0.0522 m s^{-2}
c_i	Inlet internal wave speed	0.723 m s^{-1}
r_i	Inlet Rossby radius	7.71 km
ν	Background viscosity	5×10^{-6} m^2 s^{-1}
C_a	Smagorinsky coefficient	0.1
τ	Scaled transport	0.0180
K_i	Inlet Kelvin number	1.56
Re	Reynolds number	1.45×10^6
F_i	Inlet Froude number	0.00577
α	Shelf bottom slope	2×10^{-3}
ϵ	Scaled tidal amplitude	0

the structure of the standard case that serves as a reference for these variations.

4. Plume properties

a. The standard case

For the standard case parameter values were selected that characterize a midsized coastal buoyancy source at midlatitude. The inlet volume transport is $T_i = 500$ m^3 s^{-1} and the inlet breadth is $b = 12$ km. The inlet salinity is 25, typical of an estuarine source. Table 1 shows a complete list of both dimensional and dimensionless parameters. The scaled inlet transport is $\tau = 0.018$, so the inlet transport is small compared to the geostrophic transport. The inlet Kelvin number is $K_i = 1.56$, implying that Coriolis force will have a strong influence. The inlet Froude number is $F_i = 0.00577$. The small value indicates that the inflow contributes primarily potential, not kinetic, energy. The shelf bottom slope is $\alpha = 2 \times 10^{-3}$, typical of wide shelves such as the U.S. east coast. Shelf tides are absent; only buoyancy forcing is active. The Reynolds number based on the background viscosity is Re $= 1.45 \times 10^6$ and $C_a = 0.1$.

The model was run forward in time for 166 days. By about 100 days the structure downshelf of the inlet became quasi-stationary, implying a balance then between advection and diffusion of buoyancy. Figure 2 shows the surface map of the salinity anomaly s at 166 days, where

$$s = \frac{S_a - S}{S_a - S_i}.$$

The surface isopleth where $s = 0.05$ will be defined as the effective boundary of the plume. From offshore of the inlet to its downshelf intersection with the coast, this boundary shows a plume gradually tapering in across-shelf width and convoluted with wavelike perturbations on the scale of the inlet Rossby radius, $r_i = 7.7$ km. These perturbations are likely due to flow instability, such as Yankovsky and Chapman (1997) found, and probably contribute to the effective mixing between plume and ambient shelf water. Most of this structure has the form of a buoyancy-driven coastal current.

Figure 3 shows the salinity anomaly and alongshelf current fields in a vertical, across-shelf section at $x = 440$ km, or about 60 km downshelf of the inlet. The structure is typical of a buoyancy-driven coastal current. Note the strong vertical shear, about 5×10^{-3} s^{-1}, consistent with the geostrophic shear estimated from the horizontal density gradient (6×10^{-3} s^{-1}). The alongshelf flow divides into two layers with the upper layer flowing downshelf at speeds up to 8 cm s^{-1}, while the lower layer flows upshelf toward the inlet with speed up to 3 cm s^{-1}. The total volume transports (not shown) in each layer for $0 < y < 12$ km are of the order 2000 m^3 s^{-1} in magnitude with the net transport about 250 m^3 s^{-1}, half the inlet flow of 500 m^3 s^{-1}.

At about $x = 640$ km, the plume boundary terminates (see Fig. 2). I term this point the downshelf penetration scale x_p, the property of primary interest in this study. It indicates the extent of downshelf penetration by the plume.

To provide a systematic, objective method for estimating the penetration distance x_p, I made use of the

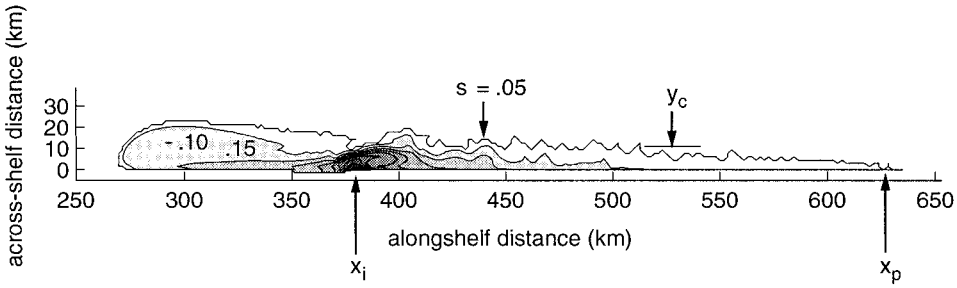

FIG. 2. Map of surface salinity anomaly s for the standard case. The time is 166 days after flow initiation. The outermost contour line is for the plume boundary, $s = 0.05$. The model domain was from $x = 0$ to $x = 785$ km; only a portion is shown here. The inlet centerline was at $x = x_i = 381$ km, while the alongshelf penetration distance was $x_p = 641$ km. The average coastal current width, y_c, was 9.7 km.

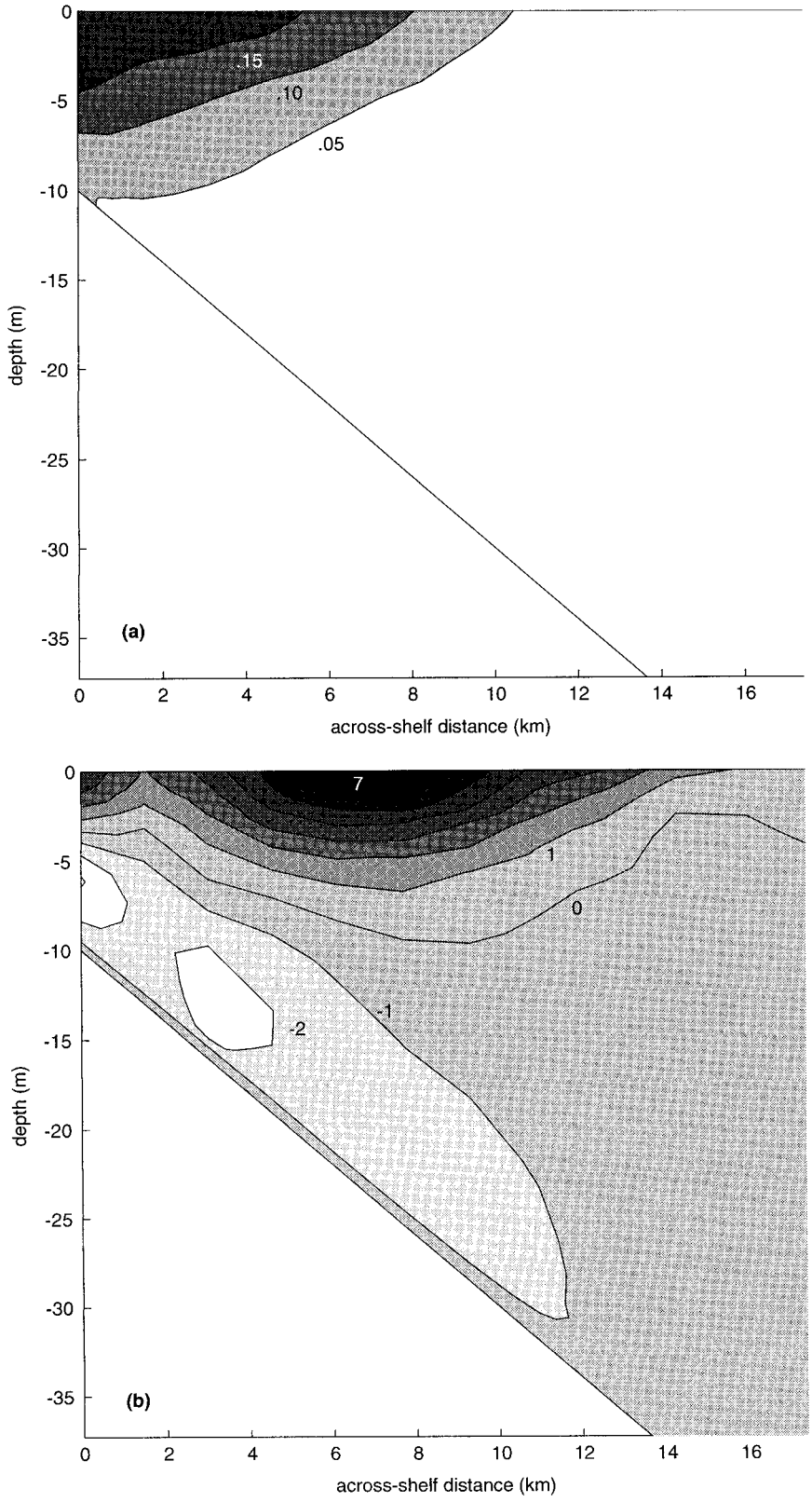

FIG. 3. Vertical sections through the coastal current for the standard case at $x = 440$ km (a) Salinity anomaly s and (b) alongshelf velocity u (cm s^{-1}).

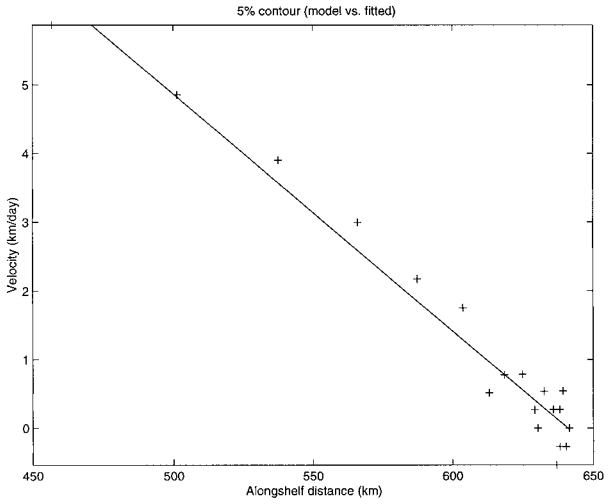

FIG. 4. Illustration of the objective method for estimating penetration distance x_p. Plus signs show data points from the model for alongshelf velocity of the plume downshelf boundary vs alongshelf distance at 8.3-day intervals. The straight line shows the linear, least squares fit. Here x_p is selected as the x value where the fitted line crosses zero velocity, 641 km.

nearly linear relation between $x(t)$ and dx/dt, where x here represents the downshelf coordinate of the intersection of the plume boundary ($s = 0.05$) at the surface and the coast. [Griffiths and Hopfinger (1983) and Whitehead and Chapman (1986) used a similar method.] Figure 4 shows a plot for the standard case. The ''plus'' symbols show the observed dependence of x versus dx/dt at 8.3-day intervals over the 166-day model run, while the straight line shows the corresponding linear fit. Interpolating the straight line to where $dx/dt = 0$ serves to estimate the value $x = x_p$, corresponding to the arrest of the plume's downshelf motion. For the fit shown in Fig. 4, $x_p = 641$ km.

The linear fit implies the differential equation

$$\frac{dx}{dt} = ax + d.$$

The integral of this gives, with $x(0) = x_0$,

$$x(t) = \left(x_0 + \frac{d}{a}\right)e^{at} - \frac{d}{a}.$$

The increase in x with t is thus modeled as an exponential with the e-folding or decay time given by $t_e = -1/a$. It follows that $x_p = dt_e$.

By using the objective analysis method, I find $x_p = 641$ km and $t_e = 29$ days for the standard case. As the center of the inlet for this case is at $x_i = 381$ km, the net downshelf penetration is $\Delta x_p = 260$ km. Scaled penetration values of interest, then, are $\Delta x_p/r_i = 33.7$, $\Delta x_p/b = 21.7$, and $\Delta x_p/\delta = 26\,000$. Whitehead and Chapman found $\Delta x_p/r_i \approx 27$.

Between the inlet and x_p the plume boundary tapers. The extent of across-shelf penetration is defined here as y_c, the offshore coordinate of the (smoothed) coastal current at its midpoint alongshelf, $x_i + (\Delta x_p/2)$. Here y_c is about 9.7 km, or $y_c/r_i = 1.3$.

b. Upshelf penetration

The plume also penetrates upshelf, however. As the map in Fig. 2 indicates, some of the inflow turns left near the inlet and moves upshelf. Some of this is lost to the outlet, but most continues upshelf beyond the outlet, reaching as far as about 100 km from the inlet. This flow executes a right turn there and flows back downshelf, joining the downshelf directed flow off the inlet. Note that the greatest across-shelf penetration, about 25 km, is attained near the right turn. Unlike the downshelf portion of the plume, this upshelf movement does not attain a stationary condition, but continues alongshelf with time.

Such upshelf buoyant intrusions have been found in many recent model results. Chapman and Lentz (1994) found similar upshelf movement using the SPEM model. Yankovsky and Chapman (1997), using the same model, prevented upshelf plume movement by imposing a uniform ambient shelf current of 4 cm s^{-1} in the downshelf direction. Fong (1998) used the same model as the present study. He found that some ambient current is required if the upshelf portion of the plume is to reach quasi-steady state. Kourafalou et al. (1996) also used the same model. They found that for a flat shelf bottom little upshelf penetration occurred, while for even weak bottom slope (2×10^{-4}), significant penetration was present. (the same is found here; see section 6). Oey and Mellor (1993) used this model and also found no upshelf penetration on their flat-bottomed shelf. McCreary et al. (1997) used a much different model, a 1.5-layer model that included an active upper layer of finite depth and an inert, infinitely deep lower layer. Under most conditions, the inlet flow turned left, moved upshelf, and then turned right to flow downshelf as it mixed with ambient ocean water. Thus, the upshelf movement of a portion of the buoyant water on a shelf with sloping bottom is not simply an artifact of the present model, but rather is commonly found.

In contrast, observations generally show little or no upshelf movement. An exception is the study of the Changjiang (Yangtze) River plume by Beardsley et al. (1985). They found surface salinity distributions (see their Fig. 7) qualitatively like that of Fig. 2 here and postulated that the left turn of a portion of the outflow was a result of vortex line stretching as the effluent moved seaward over the downward sloping bottom.

Upshelf plume penetration, including its dynamical basis, is an important but presently unsettled matter beyond the scope of the present paper. I will, instead, focus on that portion of buoyant plumes downshelf of the inlet.

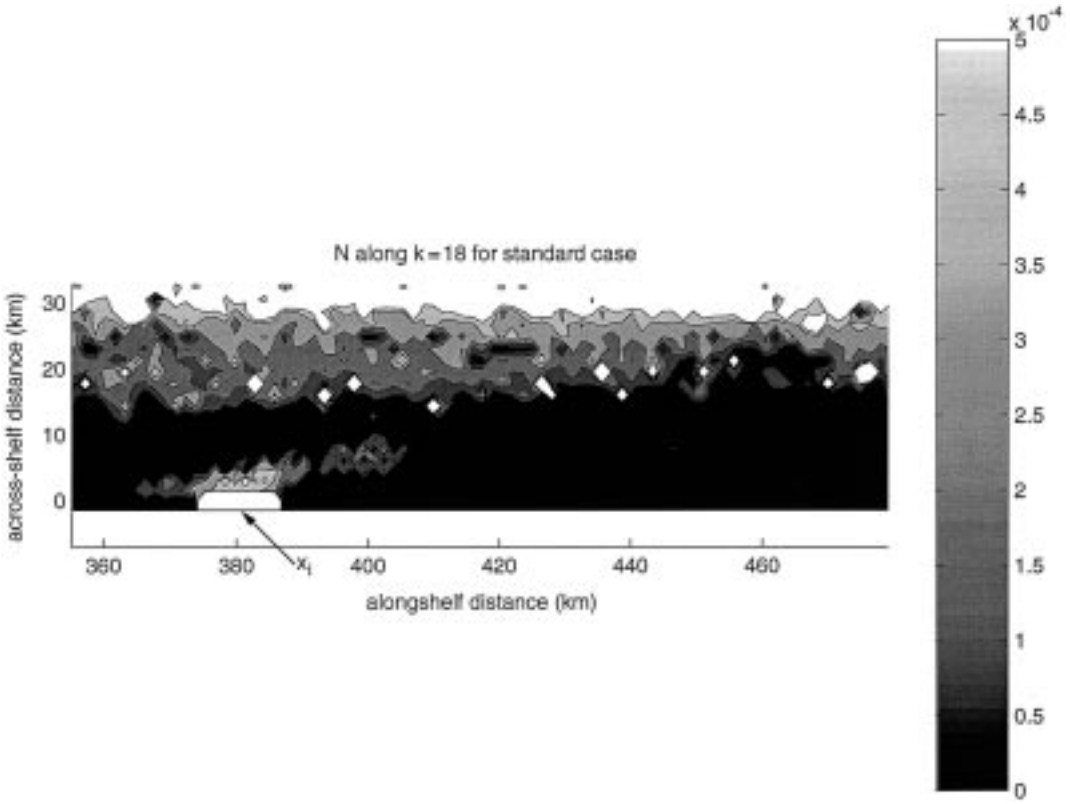

FIG. 5. Contours of vertical eddy viscosity N at intervals of 1×10^{-4} m^2 s^{-1} for the standard case along the 18th σ surface (94% of water depth). The inlet centerline is marked by x_i.

c. *Effect of the closure system*

The Mellor–Yamada level 2.5 closure system influences the results critically. Figure 5 shows a contour map of vertical eddy viscosity N over the 18th sigma surface, that is, over a planar surface at 94% of the water depth. The darkest shaded region corresponds with the location of the plume and the values of N there are less than 1×10^{-4} m^2 s^{-1}. Only well offshore and in a narrow region attached to the inlet do the levels of N rise. Furthermore, higher up in the water column and within the plume (not shown) N falls to the background level of 5×10^{-6} m^2 s^{-1}. There the Richardson number is high, for example, about 11 in the section shown in Fig. 3. The high Richardson number switches off the Mellor–Yamada closure scheme, leaving N at the background level ν, and hence leaving ν with important control of the flow field. Similar behavior of the Mellor–Yamada scheme was found in turbulent closure modeling of estuarine stratification by Nunes Vaz and Simpson (1994) and in more general applications by Burchard et al. (1998).

Alternatively, the critical role of the Mellor–Yamada scheme is made clear by repeating the same calculations for the standard case, but with $N = D = \text{const} = 1 \times 10^{-4}$ m^2 s^{-1}. The downshelf penetration is reduced in half from 260 to 130 km, while the coastal current width y_c is reduced from 9.7 to 4.1 km. Figure 6 shows the salinity anomaly and alongshelf current sections comparable to those of Fig. 3. Note the greatly decreased vertical stratification or increased isohaline slopes in the constant N case: from about 0.8×10^{-3} for closure to about 3×10^{-3} for constant N. The greater slopes are consistent with a narrower coastal current and with the greater vertical shear of the alongshelf current evident in Fig. 6b. Use of larger constant values of N leads to still greater isohaline slopes. In the present application use of the Mellor–Yamada level 2.5 closure system leads to enhanced stratification.

d. *Plume classification*

It is useful to place this plume within the context of prior classification systems for buoyant plumes. Yankovsky and Chapman (1997) classified plumes according to their vertical structure. They termed a plume as bottom advected if it remains in contact with the bottom well offshore and if its offshore boundary stretched from surface to bottom. In contrast, they termed a plume as surface advected if it has little contact with the bottom, except near shore, and if it is primarily limited to the near surface. They also recognized intermediate cases. They developed a simple criterion to predict when a

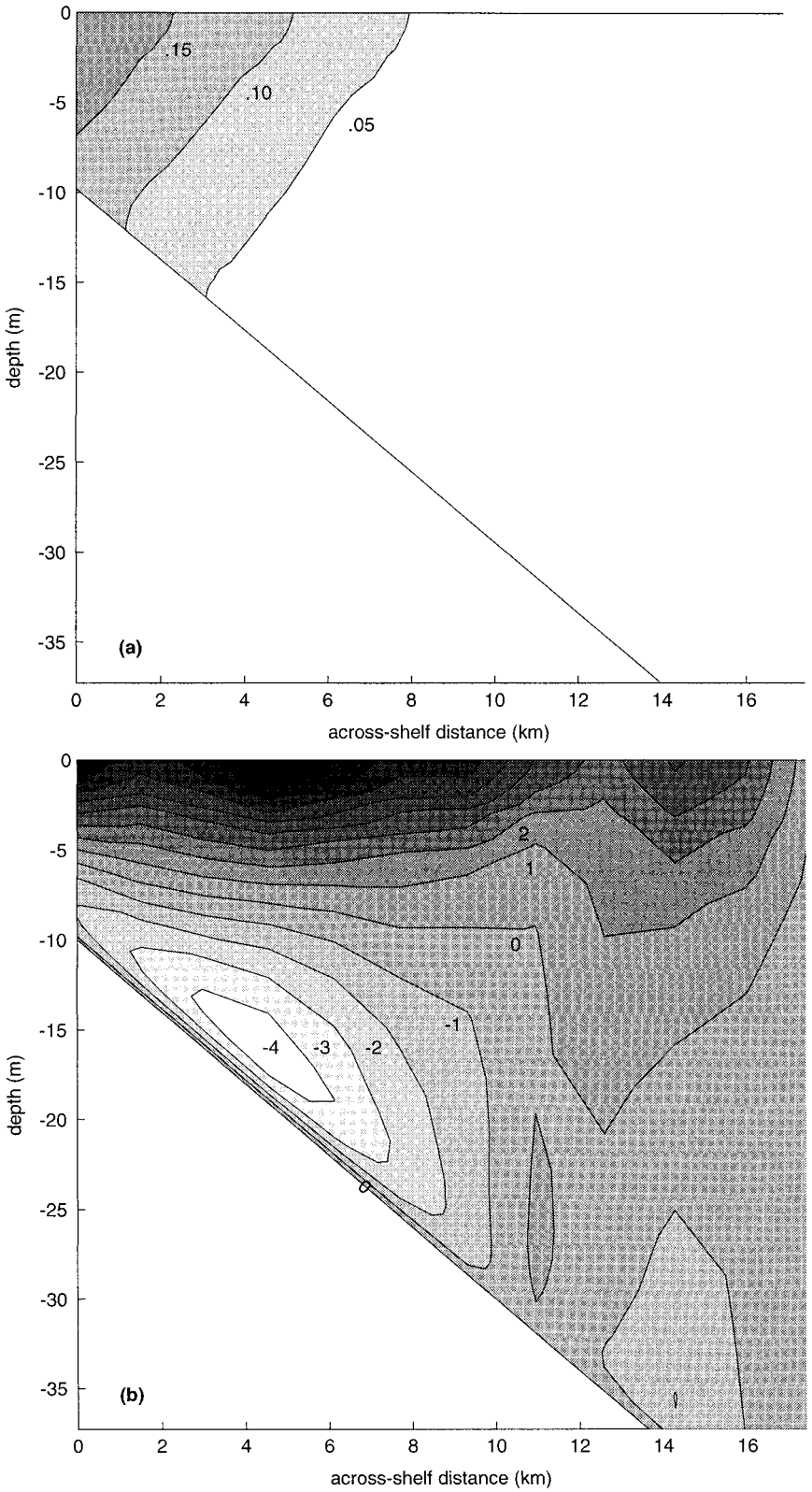

FIG. 6. As for Fig. 3 but for the standard case when $N = D = \text{const} = 1 \times 10^{-4}$ m^2 s^{-1}. (a) Salinity anomaly s and (b) alongshelf velocity u (cm s^{-1}).

TABLE 2. Parameter values for the six sets of buoyancy forced experiments.

Set	Varied parameter	Varied scaled parameter	Fixed parameters
1	$8000 < T_i < 48\,000$ m^3 s^{-1}	$1.07 < \tau < 6.41$	$K_i = 3$, Re $= 7.49 \times 10^5$
2	$100 < T_i < 28\,000$ m^3 s^{-1}	$0.00359 < \tau < 1.0$	$K_i = 1.56$, Re $= 1.45 \times 10^6$
3	$0 < f < 0.937 \times 10^{-4}$ s^{-1}	$0 < K_i < 1.56$	$F_i = 0.00577$, Re $= 1.45 \times 10^6$
4	$0.3 < b < 12$ km	$0.0389 < K_i < 1.56$	$F_i = 0.00577$, Re $= 1.45 \times 10^6$
5	$1 \times 10^{-6} < \nu < 1 \times 10^{-4}$ m^2 s^{-1}	$7.23 \times 10^4 <$ Re $< 7.23 \times 10^6$	$F_i = 0.00577$, $K_i = 1.56$
6	$1 < S_a - S_i < 6$	$0.0209 < \tau < 0.126$	none

plume is bottom-advected. In present notation this occurs when $\tau > 1$. For such a plume, the depth of the isobath at which the bottom of the offshore front is trapped is $h_b = \delta\tau^{1/2}$. For nearly all the cases studied here, $\tau < 1$, and so by their estimation these plumes are surface advected. Indeed, the same will be true of the great majority of plumes in nature with estuarine sources. Only sources having small density difference with ambient shelf water and with very high volume discharge will have $\tau > 1$ (see section 5 for examples). For the standard case, $\tau = 0.018$, so this plume should be surface advected. The limited contact of the plume with the bottom in Fig. 3 confirms this prediction.

Garvine (1995) offered a classification system for a buoyant coastal discharge based on bulk properties of the structure. The principal parameter was the bulk Kelvin number K, defined as the ratio of the plume width to the typical (not the inlet) internal Rossby radius. This system emphasized two limiting cases. The first was for small-scale plumes ($K \ll 1$) where Coriolis force played a weak role but advection of momentum was strong. The bulk Froude number then was of order one. The second was for large-scale plumes (K about 4 or greater) where the Coriolis force was primary and advection weak and Froude number small. Here we may use the results shown in Fig. 3 to estimate these parameters. The local Rossby radius is about 2.6 km and the local plume width about 10 km, so the local value of K is about 4, placing this plume in the large-scale class. The local internal wave phase speed is about 0.25 m s^{-1} while the fluid speed is about 0.04 m s^{-1}, so the local Froude number is about 0.16, consistent with the large-scale limit. In the next section cases are examined that include the small-scale limit.

5. Response to differences in buoyancy forcing

How do downshelf penetration Δx_p and coastal current width y_c change with differences in buoyancy forcing, especially differences in the inlet properties? That will be the central question of this section. In particular, for fixed shelf bottom slope α and in the absence of tidal motion ($\epsilon = 0$) I seek to find the response to changes in the parameters τ, K_i, and Re. To illustrate the striking variety of plume structure that can result from changes in these parameters, I first show results for one of the six sets of model experiments, changes caused by reduced K_i.

a. Effects of latitude change

In this set of 10 experiments the parameters are set to those of the standard case, but K_i is reduced incrementally from 1.56 to zero by reducing the latitude from 40°N to 0°. (See Table 2, set 3.) Surface salinity anomaly maps (Figs. 7 and 8) show how the horizontal plume structure changes fundamentally from midlatitudes to the Tropics. The upshelf portion of the plume is gradually transformed from a narrow region of upshelf penetration for the standard case to a wide turning region or bulge offshore of the inlet and outlet for K_i values of 0.5 and 0.2. For the equatorial plume ($K_i = 0$), the turning region has disappeared and the nonrotating dynamics now features horizontal gravitational spreading of the buoyant fluid over the ambient water. The plume shape is then symmetric alongshelf about the centerline of the inlet. These changes are accompanied by a continuous reduction in the length and width of the coastal current. For $K_i = 0.1$ only a vestige of a coastal current remains because effectiveness of the Coriolis force is weak. For $K_i = 0$ there is no coastal current.

Reduction in K_i thus causes a reduction in downshelf penetration. This is illustrated in Fig. 9 where Δx_p is plotted, scaled by inlet width b as well as by r_i. Width b is fixed at 12 km, while r_i varies from 7.71 km for the standard case to infinity for $K_i = 0$. As K_i is reduced, $\Delta x_p/b$ at first increases modestly to about 30, but then falls abruptly for $K_i < 0.3$. Meanwhile, $\Delta x_p/r_i$ falls roughly linearly with K_i to 0 at $K_i = 0$.

The plume vertical structure changes radically with K_i also. Figure 10 shows a vertical section of salinity through the centerline for the equatorial case $K_i = 0$. Where the same inlet configuration for $K_i = 1.56$ led to a coastal current penetrating downshelf (Fig. 3), now at the equator the discharged buoyant water rises quickly to form a shallow, spreading plume only about 2 m deep. The initial rise of the isopycnals just off the inlet is not resolved by the model, as it occurs in less than the grid spacing of 1.5 km. The formation of such shallow plumes for small K_i is consistent with O'Donnell's (1990) plume model that was applicable to small K_i.

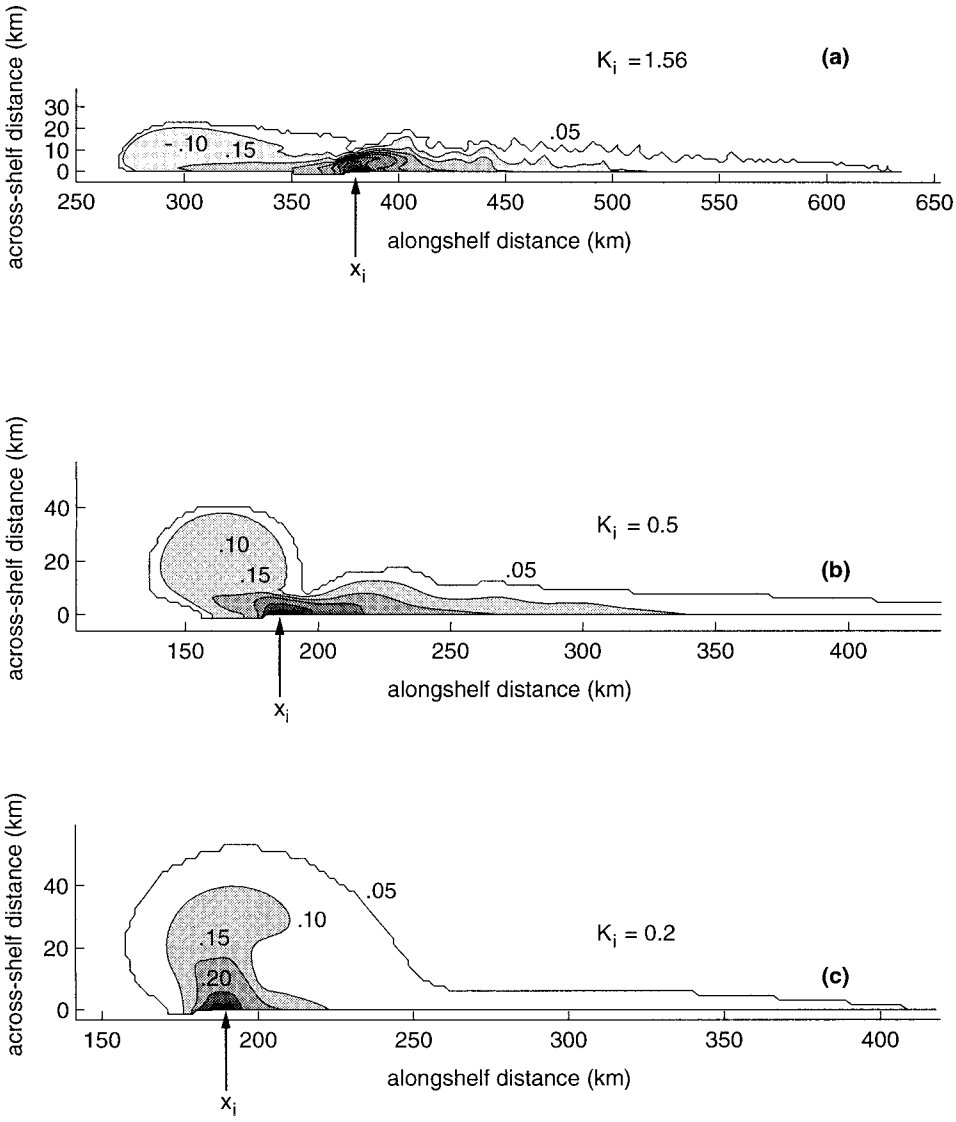

FIG. 7. Surface salinity anomaly maps for experiments with smaller source Kelvin number as a result of lower latitude. (a) The standard case $K_i = 1.56$, (b) for $K_i = 0.5$, and (c) for $K_i = 0.2$.

b. Exploration of parameter space

To explore the response of Δx_p and y_c to changes in the parameters τ, K_i, and Re I conducted six sets of experiments, each varying a single dimensional parameter systematically. The shelf bottom slope α was fixed at 2×10^{-3} and tides were absent ($\epsilon = 0$). Table 2 summarizes these experiments. Set 1 featured a strong inlet discharge T_i with the largest value 48 000 m^3 s^{-1}, typical of the Mississippi River at high discharge (Cochrane and Kelly 1986). Part of the intent here was to include plumes in the bottom-advected class of Yankovsky and Chapman (1997), that is, $\tau > 1$. Unlike the standard case, K_i was fixed at 3. Set 2 used the standard case value for $K_i = 1.56$ and also featured varied T_i, but with lower values ($100 < T_i < 28\,000$ m^3 s^{-1}). The range of τ was from 3.59×10^{-3} to 1. This set thus included the standard case. Set 3 featured K_i variations through latitude variations, as described above. Set 4 also explored K_i variations, but now by reducing inlet breadth b below that of the standard case with b as narrow as 0.3 km. Set 5 searched for the effects of the background viscosity in the Mellor–Yamada closure scheme by using a range of ν from that of molecular viscosity (1×10^{-6} m^2 s^{-1}) to 1×10^{-4} m^2 s^{-1}. Conditions otherwise corresponded to the standard case and Re ranged from 7.23×10^4 to 7.23×10^6. Finally, set 6 altered the standard case parameters by employing higher values of S_i from 26 to 31. Because c_i then varied, Re did also.

In search of a scaling rule, I attempted a scaling anal-

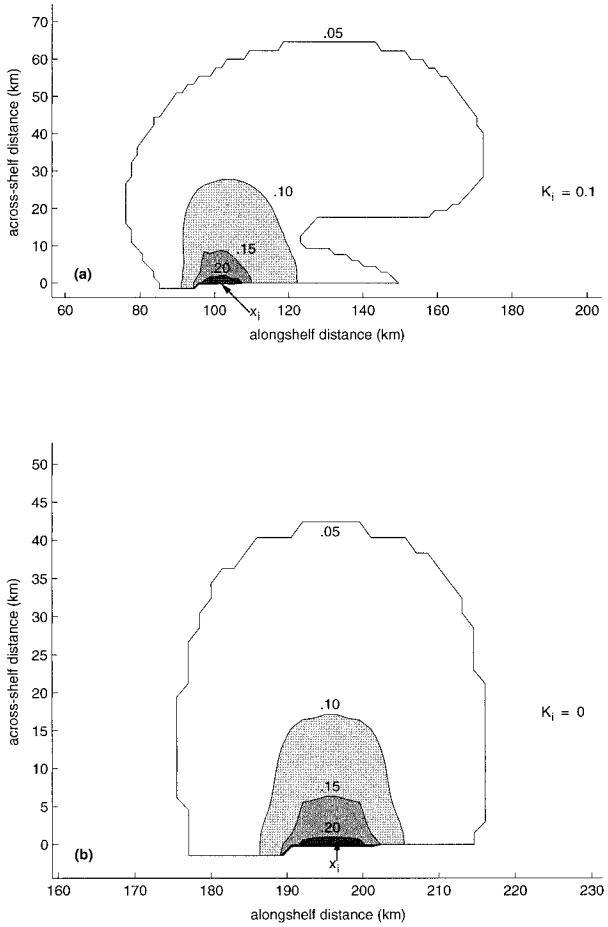

FIG. 8. As for Fig. 7 but for (a) $K_i = 0.1$ and (b) $K_i = 0$.

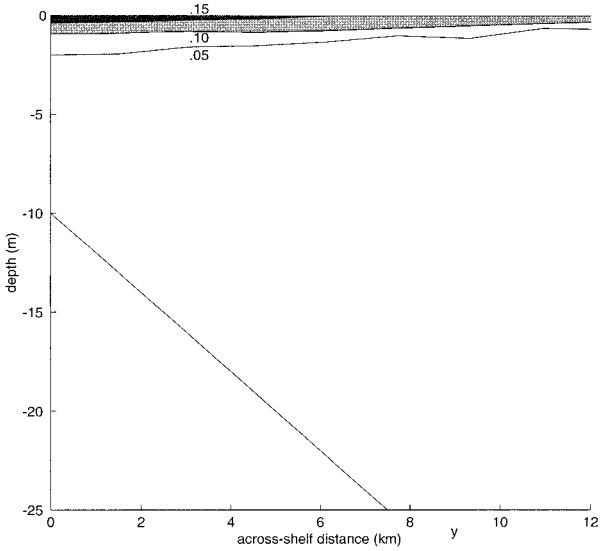

FIG. 10. Vertical section through the inlet centerline ($x = x_i$) of salinity anomaly s for the equatorial case $K_i = 0$. The inlet is at $y = 0$.

ysis for Δx_p based jointly on a simplified balance between alongshelf advection and vertical diffusion of density and on ''thermal wind balance.'' This scaling analysis was unsuccessful because there was no simple, adequate approximation for diffusivity $D = N$ that was useful over a wide range of τ. Nevertheless, this analysis did suggest normalizing Δx_p by δ.

Figure 11 shows the experimental outcome for $\Delta x_p/\delta$ plotted against τ for all six sets, a total of 44 cases. The range of τ is four orders of magnitude, from 4.5×10^{-4} to 6.4. Note the general trend for Δx_p to rise with τ.

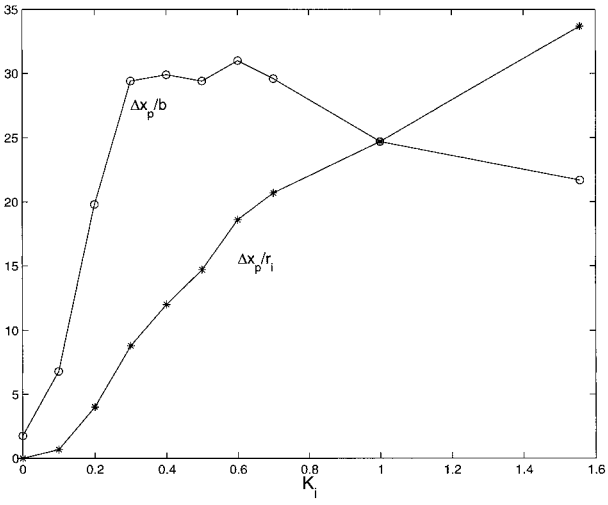

FIG. 9. Scaled downshelf penetration distance vs K_i for ten experiments at successively lower latitude. The rightmost pair of points corresponds to the standard case.

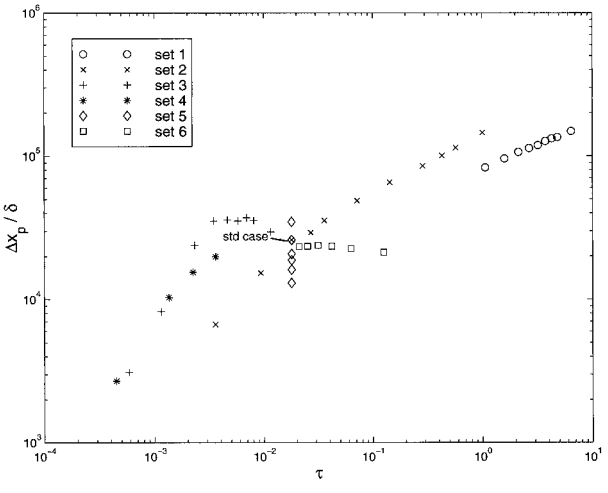

FIG. 11. Downshelf penetration distance $\Delta x_p/\delta$ for the six sets of experiments listed in Table 2 plotted against τ, the scaled inlet transport. These 44 experiments had varied buoyancy forcing properties, constant shelf bottom slope 2×10^{-3}, and no tides. The value for the standard case is noted.

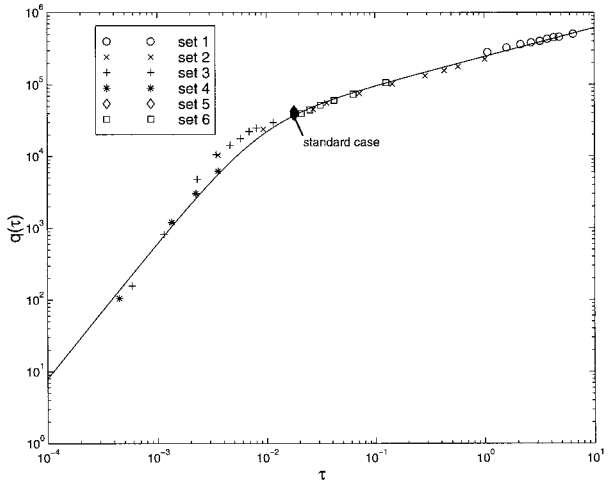

FIG. 12. Replotted data points from Fig. 11 but now for $(\Delta x_p/\delta)K_i/[1 + 0.41 \log(\mathrm{Re}/\mathrm{Re}_s)]$. The solid line shows the function $q(\tau)$ of Eq. (1) empirically fitted to these points.

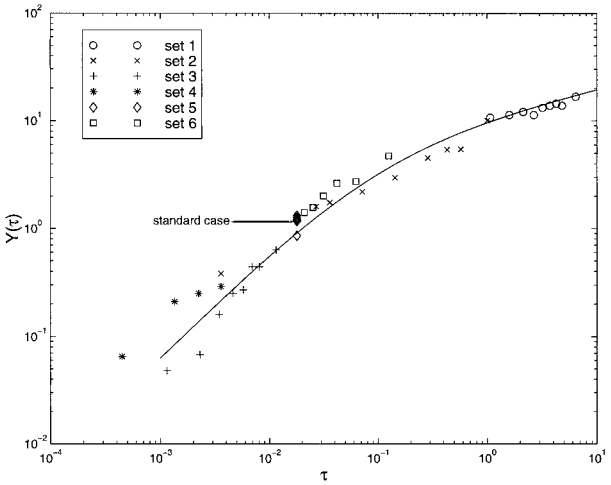

FIG. 13. Data for coastal current width y_c for the six sets of experiments of Figs. 11 and 12. The data points are for $(y_c/r_i)/[1 + 0.46 \log(\mathrm{Re}/\mathrm{Re}_s)]$ plotted against τ. The solid line shows the function $Y(\tau)$ of Eq. (2) empirically fitted to these points.

Nevertheless, there is a lot of scatter and clearly τ is not the only important dimensionless parameter.

Lacking a scaling rule, I sought to collapse most of the Δx_p data by trial and error onto a single curve when plotted against τ. The most successful similarity form was

$$\frac{\Delta x_p}{\delta} = K_i^{-1} q(\tau)\left[1 + 0.41 \log\left(\frac{\mathrm{Re}}{\mathrm{Re}_s}\right)\right]. \qquad (1)$$

Here $\mathrm{Re}_s = 1.45 \times 10^6$, the standard case value for Re and log is the base 10 logarithm; $q(\tau)$ is a dimensionless, empirical function of τ alone to be obtained by fitting an analytic function to a plot of $(\Delta x_p/\delta)K_i/[1 + 0.41 \log(\mathrm{Re}/\mathrm{Re}_s)]$ versus τ.

The data for this plot appear in Fig. 12. The scatter of Fig. 11 is now greatly reduced. The single curve fitted to these data appears as the solid line in Fig. 12 and is given analytically by

$$q(\tau) = \frac{3.16 \times 10^8 \tau^{1.90}}{1 + 1288\tau^{1.50}}.$$

For $\tau \ll 10^{-2}$, $q(\tau) \cong 3.16 \times 10^8\ \tau^{1.90}$, while for $\tau \gg 10^{-2}$, $q(\tau) \cong 2.45 \times 10^5\ \tau^{0.40}$. Consequently, for small τ, $\Delta x_p/\delta$ varies as $\tau^{1.9}$, while for large τ, $\Delta x_p/\delta$ varies more slowly as $\tau^{0.4}$.

For fixed K_i and τ, $\Delta x_p/\delta$ still varies with the background viscosity through Re. Suppose that because of enhanced internal wave activity, the background viscosity were 2×10^{-5} rather than 0.5×10^{-5} m^2 s^{-1}, as used for the standard case. Then Δx_p would be reduced by the factor 0.75.

The transformation of the scattered results for Δx_p in Fig. 11 into the empirical expression of Eq. (1) represents the attainment of dynamic similarity (Kundu 1990) for downshelf penetration. In fluid mechanics two flow fields are said to be dynamically similar if their governing dimensionless parameters are equal, even though their dimensional parameters differ. For the present case the similarity parameters are τ, K_i, and Re.

A similar attempt at collapsing data for the coastal current width y_c was less successful, but still useful. As buoyancy-driven coastal currents are all products of earth rotation, it is useful to scale their widths by r_i. The similarity form

$$y_c/r_i = Y(\tau)[1 + 0.46 \log(\mathrm{Re}/\mathrm{Re}_s)], \qquad (2)$$

was adopted here, where the factor in brackets provides adjustment for background ν. In parallel with Fig. 12 for Δx_p, data for Y are plotted in Fig. 13. The data collapse well to a single curve except when $\tau < 0.004$ where much scatter remains. This is the range where one would expect complexity, for as τ becomes small, rotation effects diminish and coastal currents disappear, as in Fig. 8. The fitted curve for $Y(\tau)$ that is plotted is thus useful for $\tau > 0.004$ and has the analytic form

$$Y(\tau) = \frac{65\tau}{1 + 5.8\tau^{0.75}}.$$

A particular value of interest is $\tau = 1$, the lower bound for the Yankovsky and Chapman (1997) bottom-advected plumes. For $\tau = 1$, then, Eq. (2) gives $y_c = 9.6r_i$ if $\mathrm{Re} = \mathrm{Re}_s$. For $\tau > 1$, $Y(\tau) \cong 11.2\tau^{0.25}$, so then y_c increases only slowly with τ.

The six sets of experiments were all conducted with the Smagorinsky coefficient C_a fixed at 0.1. Flow fields with this value had a plausible amount of fine structure, while those with C_a lowered to 0.02 had excessive structure and those with C_a raised to 1.0 were excessively smoothed. As noted earlier, horizontal diffusivity does contribute to the mixing that selects Δx_p. To show the amount of sensitivity in Δx_p to the choice of C_a, I recomputed the standard case with C_a ranging from 0.02

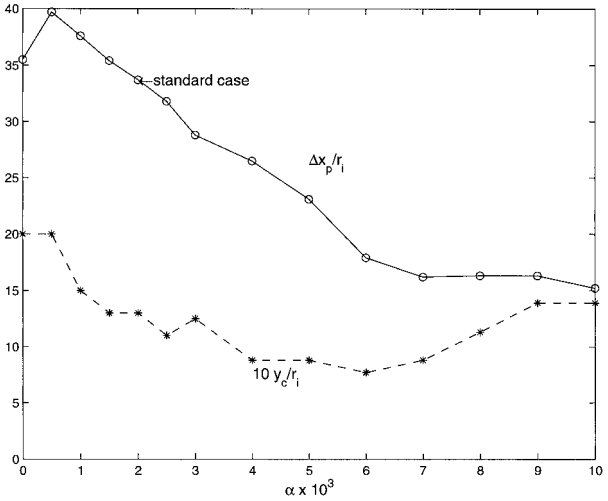

FIG. 14. Downshelf penetration distance and coastal current width plotted against shelf bottom slope α for 14 experiments, including the standard case. Note the scale factor of 10 applied to y_c/r_i data.

to 1. Values for $\Delta x_p/r_i$ ranged from 49 to 10, respectively, and the results were well fitted by the log-linear relation

$$\Delta x_p/r_i = 10 - 23.5 \log C_a.$$

Thus, doubling or halving C_a will change $\Delta x_p/r_i$ by the amount 23.5 log2 = 7.1, a substantial, but not dominating change.

6. Response to varied ambient conditions

In this section the two properties of the ambient shelf are varied, the bottom slope and tidal amplitude, that were fixed at 2×10^{-3} and zero, respectively, for the standard case and the experiments of section 5.

a. Bottom slope effects

Figure 14 shows the outcome of a series of 13 model runs with parameters set to those of the standard case, except for bottom slope α. In general, the penetration downshelf, $\Delta x_p/r_i$, decreases for increased α over the range from 0.5×10^{-3} to 10×10^{-3}. As the latter slope is approached, the results suggest an asymptotic limit for $\Delta x_p/r_i$ of about 16, considerably lower than the peak value of about 35 for the weak slope cases, including zero slope. In contrast, coastal current width y_c/r_i shows an initial decrease from about 2 to 1, but then it recovers to about 1.5 for larger slope.

The flat-bottomed shelf is of special interest because it shows little upshelf penetration, in contrast to all other cases. Now $h = \delta = 10$ m everywhere. Figure 15 shows the surface salinity anomaly for zero slope as well as that of the standard case for which $\alpha = 2 \times 10^{-3}$. This result is similar to that found by Kourafalou et al. (1996) and Oey and Mellor (1993) for $\alpha = 0$. Thus, it appears that upshelf penetration in these models and the present model involves vortex line stretching of water in contact with the bottom, as that mechanism disappears with zero slope.

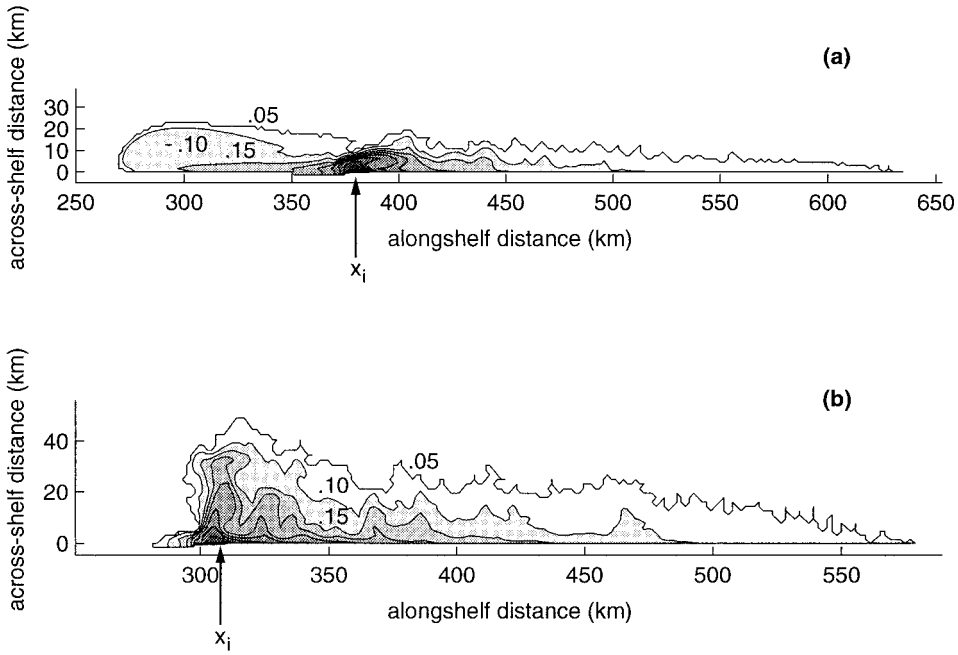

FIG. 15. Surface salinity anomaly maps for (a) the standard case ($\alpha = 2 \times 10^{-3}$) and (b) for the flat-bottomed shelf ($\alpha = 0$).

b. Shelf tidal effects

We may expect the presence of barotropic tidal motion on the shelf to impose a variety of mechanisms on a buoyant plume that affect its across-shelf and downshelf penetration. These effects include enhanced vertical mixing (tidal mixing), principally through elevated bottom stress, tidal straining of the stratified flow of the plume (Simpson and Souza 1995), and advection of plume water by nonlinearly induced subtidal frequency flow (Ianniello 1977; and Tee 1980).

Barotropic tidal forcing was introduced in the model by imposing surface elevation variations with time at the model seaward boundary as

$$\eta(t) = A \cos(2\pi t/P),$$

where P is the M_2 tidal constituent period and A is the elevation amplitude. (The normalized amplitude is $\epsilon = A/\delta$.) This form imposes a simple in-phase cooscillating tide at the boundary.

To check that the model created correct tidal currents, I ran it with the standard case settings, but with $T_i = 0$, that is, with uniform density ρ_a. Rotary shelf tidal currents resulted that had their principal axes oriented nearly across-shelf and that were uniform alongshelf, indicating that the ''smooth'' boundary conditions used for the open, across-shelf boundaries did not introduce artifacts.

Battisti and Clarke (1982) provided a simple, analytical barotropic shelf tidal model that is applicable here. For weak bottom friction and no phase variation alongshelf, their tidal model gives

$$V_t = A\sigma/\alpha, \tag{3}$$

where V_t is the across-shelf, vertically averaged tidal current amplitude and $\sigma = 2\pi/P$ is the tidal frequency for M_2. The corresponding alongshelf current amplitude is $U_t = V_t f/\sigma$.

The present model reproduced these currents well, although near the coastal wall the across-shelf current amplitude fell lower. Figure 16 shows an example for $A = 4$ m of the time series upshelf of the inlet at midshelf ($y = 20$ km) for the across-shelf surface velocity. Note the transient behavior. For the first several tidal periods the current amplitude is over 1 m s^{-1} and high frequency fluctuations are present. After about 20 tidal periods the transient behavior ends. Then the motion has only a harmonic variation at M_2 with amplitude 27 cm s^{-1}. The alongshelf current amplitude there is 19 cm s^{-1}. The corresponding amplitudes from the Battisti and Clarke model are 28 and 19 cm s^{-1}, respectively.

Figure 17 shows an example of the tidal effects on the surface salinity anomaly field for amplitude $A = 4$ m or $\epsilon = 0.4$. Compared to the standard case ($\epsilon = 0$, upper panel), there are two notable differences. First, upshelf penetration is reduced with tides. Second, downshelf penetration is reduced compared to the standard case, but across-shelf penetration is unchanged.

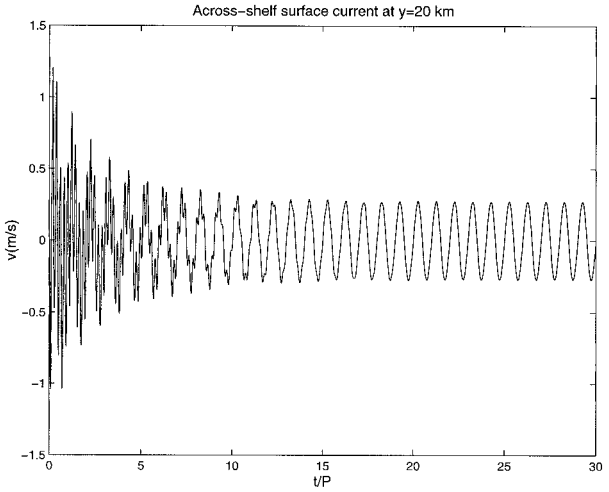

FIG. 16. Surface current across-shelf component v at midshelf ($y = 20$ km) for the standard case, but with imposed tidal height amplitude 4 m ($\epsilon = 0.4$); v is shown as a time series from initiation of tidal motion ($t = 0$) to 30 M_2 tidal periods ($t/P = 30$).

Figure 18 summarizes the downshelf penetration for nine cases. The range of tidal amplitude parameter is from $\epsilon = 0$ (the standard case) to $\epsilon = 0.4$, the upper level for shelf tidal amplitudes, roughly corresponding to M_2 tides in the Bay of Fundy or the northwest European shelf. Across-shelf penetration y_c/r_i changes little and is not shown. Downshelf penetration falls nearly linearly with increased ϵ from the standard case level of $\Delta x_p/r_i = 33.7$ to 15.3 at $\epsilon = 0.4$, or 45% of the standard case values. Shelf tides thus have a detectable but moderate influence on plume downshelf penetration.

7. Concluding remarks

The major objective of this study was to find the dependence of the penetration of a buoyant coastal discharge, both downshelf and across-shelf, upon fundamental parameters. For this purpose the three-dimensional, primitive equation model ECOM3d was used, a variant of the Princeton Ocean Model (Blumberg and Mellor 1987). To focus on fundamentals I used an idealized setting that included a straight coast with constant shelf bottom slope. Buoyant water entered the shelf through an inlet in the coastal wall. Ambient shelf conditions included tidal motion, but neither wind stress nor ambient alongshelf currents. Both of these latter agents will affect downshelf penetration. The flow began from a state of rest after switching on the buoyant source at the coast and tidal elevation variations at the offshore boundary. Results were analyzed after attainment of a nearly stationary state for the downshelf part of the plume.

Five independent, dimensionless parameters determined the plume's penetration. The scaled volume transport of the source, τ, controls the greatest variance. The other parameters are the source Kelvin number K_i, the

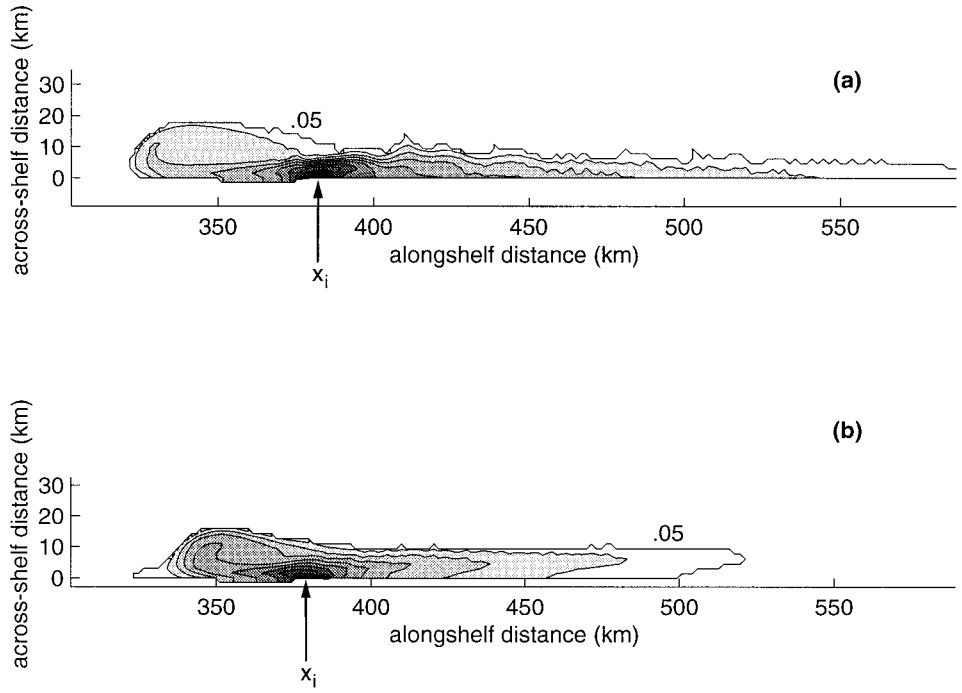

FIG. 17. Surface salinity anomaly maps for (a) the standard case (no tides) and (b) for $\epsilon = 0.4$.

Reynolds number Re based on the background eddy viscosity ν, the shelf bottom slope α, and the scaled tidal amplitude ϵ.

To explore this parameter space I made 66 separate model runs in groups of related experiments. For fixed α and without tides, an empirical similarity form for the downshelf penetration Δx_p was found:

$$\frac{\Delta x_p}{\delta} = K_i^{-1} q(\tau)\left[1 + 0.41 \log\left(\frac{\mathrm{Re}}{\mathrm{Re}_s}\right)\right],$$

where an analytic expression for $q(\tau)$ was found by fitting the experimental points. This similarity form is valid over four orders of magnitude for τ, including tropical plumes and plumes that are bottom-advected in the classification of Yankovsky and Chapman (1997) for which $\tau > 1$. A similarity form also resulted for the mean width of the coastal current y_c, scaled by the inlet Rossby radius r_i.

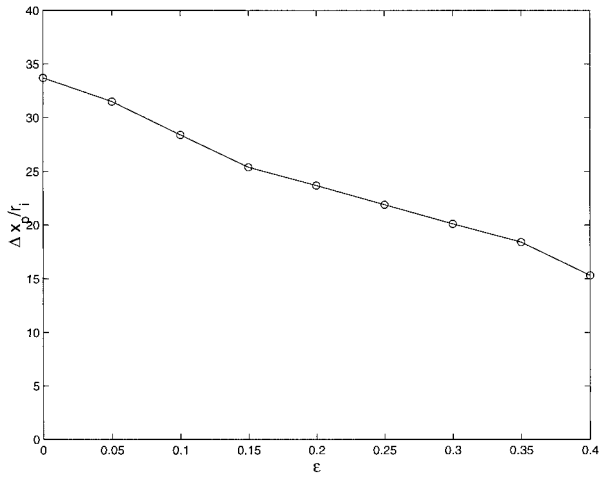

FIG. 18. Downshelf penetration distance plotted against the tidal parameter ϵ.

In other experiments α was varied. Downshelf penetration fell by a factor of about 2 when the slope increased from the order 10^{-3} to 10^{-2}. Moderate reductions were also produced by adding tidal motion. Over the expected full range of shelf tidal elevation amplitude ($0 < \epsilon < 0.4$), $\Delta x_p/r_i$ fell from 33.7 to 15.3, a reduction to about 45%.

To illustrate application of the similarity forms to predicting penetration for natural cases, consider two cases where there are adequate source data: the Delaware coastal current (Münchow and Garvine 1993) and the Labrador Current (Lazier and Wright 1993). Münchow and Garvine measured source buoyancy flux levels of $g'T_i = 100\ \mathrm{m^4\ s^{-3}}$ and $g' = 0.03\ \mathrm{m\ s^{-2}}$, or $T_i = 3300\ \mathrm{m^3\ s^{-1}}$. The source depth δ was about 10 m, while $f = 0.9 \times 10^{-4}\ \mathrm{s^{-1}}$. Thus, r_i was about 6.1 km. The source breadth was $b = 8$ km. Bottom slope α is about 1×10^{-3} and shelf tidal amplitude A is about 0.5 m. Consequently, $\tau = 0.20$, while $K_i = 1.3$. With $\nu = 5 \times 10^{-5}\ \mathrm{cm^2\ s^{-1}}$, $\mathrm{Re} = 1.10 \times 10^5$. The scaled tidal amplitude is $\epsilon = 0.05$. We first ignore tides and use the results of section 5. For $\tau = 0.20$, $q = 1.3 \times 10^5$. Upon substituting these in Eq. (1) we find $\Delta x_p = 530$ km. From Fig. 18 the fractional reduction of Δx_p for $\epsilon =$

0.05 is estimated to be about 0.93 or, with tides, $\Delta x_p \cong$ 500 km. This distance exceeds the alongshelf separation of the source, Delaware Bay, from the nearest, large neighboring source downshelf, Chesapeake Bay. Thus, the model results predict that the Delaware coastal current should often merge with the Chesapeake plume. The Delaware coastal current was mapped to its merger with the Chesapeake in April 1993 (T. Sanders 1998, personal communication). From section 5 we find $Y =$ 4.8, so that Eq. (2) predicts $y_c = 14$ km. The observed value for April 1993 was 15 km.

Lazier and Wright (1993) state that the Labrador Current is a continuation of its primary source, the Baffin Island Current (LeBlond et al. 1981). It transports cold, low salinity, low density water southward over the continental shelf and slope of Labrador. (This current is distinct from the deep Labrador Current, a western boundary current below 2000-m depth.) Chapman and Beardsley (1989) hypothesized that the Labrador Current, supplemented by other coastal buoyancy sources to the south, is the origin for the shelf water of the Middle Atlantic Bight. They suggest that these northern low salinity waters form a buoyancy-driven coastal current over 5000 km in length, reaching to the southern end of the Middle Atlantic Bight at Cape Hatteras. Here the source properties given by Lazier and Wright are used together with the model results to obtain the scales for penetration. Since the natural setting includes complex topography and numerous changes in coastline orientation, only the scales are relevant. Lazier and Wright estimate the source volume transport at $T_i = 2.7$ Sv (Sv $\equiv 10^6$ m^3 s^{-1}), while their Fig. 15a shows $\delta = 200$ m and $b = 120$ km. Source density ρ_i is about 1025.5 kg m^{-3}, while $\rho_a = 1027$ kg m^{-3}, so that $g' = 0.14$ m s^{-2}. Bottom slope for the Labrador shelf is about 2×10^{-3} and $f = 1.3 \times 10^{-4}$ s^{-1}. Thus, $r_i = 13$ km, and $K_i =$ 9.2. Scaled transport is large at $\tau = 1.2$. With $\nu = 5 \times 10^{-5}$ m^2 s^{-1} again, Re $= 6.8 \times 10^6$ and $q(\tau) = 2.66 \times 10^5$, giving $\Delta x_p = 7400$ km. Tidal action would shorten this somewhat. The scale of the model downshelf penetration thus is consistent with the Chapman and Beardsley hypothesis. The model scale for the coastal current width using Eq. (2) is 175 km, roughly the width of the Labrador continental shelf.

The experiments with the numerical model presented have been successful in coping with a large range of model parameters, especially in the primary parameter τ that ranged over four orders of magnitude. Nevertheless, the sensitivity of penetration values to model mixing parameters is cause for caution. Frequently, over much of the plume body the high stratification or large Richardson number caused the Mellor–Yamada level 2.5 turbulent closure scheme to switch off, leaving the vertical diffusion at the selected (and therefore arbitrary) background level ν. Nunes Vaz and Simpson (1994) and Burchard et al. (1998) found similar behavior with Mellor–Yamada schemes in their models. In the present model this led to significant, though not crucial, dependence of penetration upon ν. In section 5, experiment set 5 for example (Fig. 11), as ν was changed from that of the standard case (0.5×10^{-5} m^2 s^{-1}) to the molecular value (0.1×10^{-5}), Δx_p increased by 34%, while when ν was increased to 10×10^{-5}, Δx_p decreased by 50%. Meanwhile, the low levels for vertical diffusivity within the plume left opportunity for some mixing to be accomplished by the lateral diffusivity of the model. Variation of the coefficient C_a used in the Smagorinsky (1963) scheme showed a similar amount of control over Δx_p. Because objectively determined values for ν and C_a are lacking, we should regard the outcomes of calculations of Δx_p as valid only to within about a factor of 2 or 3.

Acknowledgments. J. R. Zagar contributed essential skills in numerical analysis, code development, and graphics. Alan Blumberg of HydroQual, Inc., made the code for ECOM3d available. I am indebted to Richard Signell for installing the code and for frequent advice. The original manuscript was improved through the helpful comments of David Chapman, Derek Fong, Kevin Horsburgh, Pablo Huq, Steven Lentz, Andreas Münchow, Chandra Narayanan, James O'Donnell, and two anonymous reviewers. Jacqueline Bijansky typed the manuscript. This work was supported by the National Science Foundation through Grant OCE-9503040.

REFERENCES

Battisti, D. S., and A. J. Clarke, 1982: A simple method for estimating barotropic tidal currents on continental margins with specific application to the M_2 tide off the Atlantic and Pacific coasts of the United States. *J. Phys. Oceanogr.,* **12,** 8–16.

Beardsley, R. C., R. Limeburner, H. Yu, and G. A. Cannon, 1985: Discharge of the Changjiang (Yangtze) River into the East China Sea. *Contin. Shelf Res.,* **4,** 57–76.

Blumberg, A. F., and G. L. Mellor, 1987: A description of a three-dimensional coastal ocean circulation model. *Three-Dimensional Coastal Ocean Models,* N. Heaps, Ed., Amer. Geophys. Union, 1–16.

Burchard, H., O. Petersen, and T. P. Rippeth, 1998: Comparing the performance of the Mellor–Yamada and the k-ε two equation turbulence models. *J. Geophys. Res.,* **103,** 10 543–10 554.

Chapman, D. C., and R. C. Beardsley, 1989: On the origin of shelf water in the Middle Atlantic Bight. *J. Phys. Oceanogr.,* **19,** 384–391.

——, and S. J. Lentz, 1994: Trapping of a coastal density front by the bottom boundary layer. *J. Phys. Oceanogr.,* **24,** 1464–1479.

Cochrane, J. D., and F. J. Kelly, 1986: Low-frequency circulation on the Texas–Louisiana continental shelf. *J. Geophys. Res.,* **91,** 10 645–10 659.

Epifanio, C. E., 1996: Transport of blue crab (*Callinectes sapidus*) larvae in the waters off Mid-Atlantic states. *Bull. Mar. Sci.,* **57,** 713–725.

Fong, D. A., 1998: Dynamics of freshwater plumes: Observations and numerical modeling of the wind-forced response and alongshore freshwater transport. Ph.D. thesis, MIT/WHOI Joint Program in Oceanography, 155 pp. [Available from Woods Hole Oceanographic Institution, Woods Hole, MA 02543.]

Garvine, R. W., 1987: Estuary plumes and fronts in shelf waters: A layer model. *J. Phys. Oceanogr.,* **17,** 1877–1896.

——, 1991: Subtidal frequency estuary–shelf interaction: Observations near Delaware Bay. *J. Geophys. Res.,* **96,** 7049–7064.

——, 1995: A dynamical system for classifying buoyant coastal discharge. *Contin. Shelf Res.*, **15,** 1585–1596.

Griffiths, R. W., and E. J. Hopfinger, 1983: Gravity currents moving along a lateral boundary in a rotating fluid. *J. Fluid Mech.*, **134,** 357–399.

Hickey, B. M., L. J. Pietrafesa, D. A. Jay, and W. C. Boicourt, 1998: The Columbia River plume study: Subtidal variability in the velocity and salinity fields. *J. Geophys. Res.*, **103,** 10 339–10 368.

Hill, A. E., 1998: Buoyancy effects in coastal and shelf seas. *The Sea*, Vol. 10, K. H. Brink and A. R. Robinson, Eds., John Wiley and Sons, 21–62.

Ianniello, J. P., 1977: Tidally induced residual currents in estuaries of constant breadth and depth. *J. Mar. Res.*, **35,** 755–786.

Kourafalou, V. K., L.-Y. Oey, J. D. Wang, and T. N. Lee, 1996: The fate of river discharge on the continental shelf. 1. Modeling the river plume and the inner shelf coastal current. *J. Geophys. Res.*, **101,** 3415–3434.

Kundu, P. K., 1990: *Fluid Mechanics* (chapter 8), Academic Press, 638 pp.

Lazier, J. R. N., and D. G. Wright, 1993: Annual velocity variations in the Labrador Current. *J. Phys. Oceanogr.*, **23,** 659–678.

LeBlond, P. H., T. R. Osborn, D. O. Hodgins, R. Goodman, and M. Metge, 1981: Surface circulation in the western Labrador Sea. *Deep-Sea Res.*, **28A,** 683–693.

McCreary, J. P., Jr., S. Zhang, and S. R. Shctye, 1997: Coastal circulations driven by river outflow in a variable-density 1½-layer model. *J. Geophys. Res.*, **102,** 15 535–15 554.

Mellor, G. L., and T. Yamada, 1982: Development of a turbulent closure model for geophysical fluid problems. *Rev. Geophys. Space Phys.*, **20,** 851–875.

Mork, M., 1981: Circulation phenomena and frontal dynamics of the Norwegian coastal current. *Philos. Trans. Roy. Soc. London*, **302A,** 635–647.

Münchow, A., and R. W. Garvine, 1993: Buoyancy and wind forcing of a coastal current. *J. Mar. Res.*, **51,** 293–322.

Nunes Vaz, R. A., and J. H. Simpson, 1994: Turbulence closure modeling of estuarine stratification. *J. Geophys. Res.*, **99,** 16 143–16 160.

O'Donnell, J., 1990: The formation and fate of a river plume: A numerical model. *J. Phys. Oceanogr.*, **20,** 551–569.

Oey, L.-Y., and G. L. Mellor, 1993: Subtidal variability of estuarine outflow, plume, and coastal current: A model study. *J. Phys. Oceanogr.*, **23,** 164–171.

Simpson, J. H., and A. J. Souza, 1995: Semidiurnal switching of stratification in the region of freshwater influence of the Rhine. *J. Geophys. Res.*, **100,** 7037–7044.

Smagorinsky, J., 1963: General circulation experiments with the primitive equations, 1. The basic experiment. *Mon. Wea. Rev.*, **91,** 99–164.

Smolarkiewicz, P. K., and W. W. Grabowski, 1990: The multidimensional positive definite advection transport algorithm. *J. Comput. Phys.*, **86,** 355–375.

Tee, K.-T., 1980: The structure of three-dimensional tide-induced current. Part II: Residual currents. *J. Phys. Oceanogr.*, **10,** 2035–2057.

Whitehead, J. A., and D. C. Chapman, 1986: Laboratory observations of a gravity current on a sloping bottom: The generation of shelf waves. *J. Fluid Mech.*, **172,** 373–399.

Yankovsky, A. E., and D. C. Chapman, 1997: A simple theory for the fate of buoyant coastal discharges. *J. Phys. Oceanogr.*, **27,** 1386–1401.

Ye, J., and R. W. Garvine, 1998. A model study of estuary and shelf tidally driven circulation. *Contin. Shelf Res.*, **18,** 1125–1155.